An Aperiodic mm-Wave Phased Array Controlled by Multi-Channel Analog Beamforming ICs

Buenaventura-Camps, Marta; Aslan, Yanki; Freidl, Philipp; Aubry, Pascal; Onat, Nehir Berk; Janssen, Johan; Geurts, Marcel; Yarovoy, Alexander

DOI
10.23919/EuMC61614.2024.10732229

Publication date
2024

Document Version
Final published version

Published in
2024 54th European Microwave Conference, EuMC 2024

An Aperiodic mm-Wave Phased Array Controlled by Multi-Channel Analog Beamforming ICs

Marta Buenaventura-Camps[#$], Yanki Aslan[$], Philipp Freidl[*], Pascal Aubry[$], Nehir Berk Onat[$], Johan Janssen[*], Marcel Geurts[*], Alexander Yarovoy[$]

[#]Robin Radar Systems, The Netherlands
[$]Microelectronics Department, Delft University of Technology, The Netherlands
[*]NXP Semiconductors, The Netherlands
mbuenaventurac@gmail.com, {y.aslan, p.j.aubry, n.b.onat, a.yarovoy}@tudelft.nl,
{philipp.freidl, johan.janssen, marcel.geurts}@nxp.com

***Abstract* — A novel dual-linear polarized active aperiodic millimeter-wave (26 GHz band) phased array is prototyped. Four-channel integrated circuits are used for beamforming. An asymmetrical signal distribution and antenna feeding network is designed. A heuristic post-calibration method is applied in beam steering. The measurements show that, as compared to the benchmark array with a conventional square-grid layout, the proposed aperiodic topology can significantly decrease the peak sidelobe level, the extent of which depends on the polarization and scan angle. This comes at the expense of larger array size, higher feed network losses and increased cross-polarization levels.**

***Keywords* — active antenna, antenna layout, aperiodic array, beamforming, integrated circuit, millimeter-wave, phased array.**

I. Introduction

Uniform-amplitude aperiodic arrays have a high potential of achieving low sidelobes at optimal power efficiencies via spatial tapering [1]. Different topology optimization strategies have been discussed in the literature from a mathematical perspective [2]. However, the practical design of the resulting phased array layouts in today's multi-channel integrated circuit IC technology [3], [4] has not yet been considered, except some thinned or clustered arrays [5], [6]. In the case of a fully aperiodic array layout, there is a significant circuit routing challenge on the radio frequency (RF) signal distribution network and IC-to-antenna element feed lines, which also brings serious calibration needs [7]. There are a few recent theory-level discussions on antenna clustering and mapping algorithms [8], [9], but, to the authors' knowledge, there is no prior work on practical non-regular distribution of the ICs and the realization of an asymmetrical feed network.

In this article, partly conducted as a M.Sc. thesis project at TU Delft [10], we propose a novel innovative aperiodic-layout IC-integrated dual-polarized phased array system prototype (in Fig. 1b) with experimental verification. We re-use as many components as possible (antenna element, IC, feed line, heat sink) from a reference regular array [11], [12] (in Fig. 1a) used as benchmark to highlight the benefits of the new topology.

The rest of this article is organized as follows. Section II describes the array system components and the post-manufacturing calibration approach. Section III presents the measurement results. Section IV concludes the article.

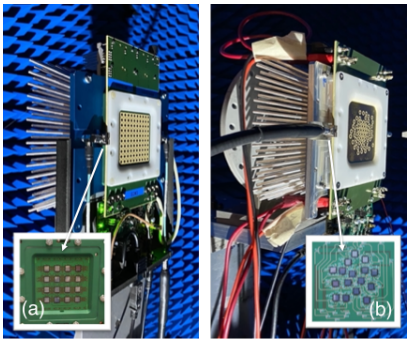

Fig. 1. 64-element 26 GHz array: (a) square-grid [11], (b) aperiodic (new).

II. Array System Development

A. Board Stack-Up

The board stack-up consists of 12 layers, as shown in Fig. 2. Astra MT77, with a dielectric constant of 3 for the core substrate and 2.95 for the pre-preg, is used as the dielectric material for the printed circuit board (PCB). The upper layers are dedicated to the antennas and are separated from the rest of the subsystems by layer M6, which includes the ground plane for the antenna array and ensures its independent design. The layers beneath M6 contain the routing for the feeding network, control signals, and the analog beamforming ICs at the bottom.

B. Beamforming IC

The MMW9014K 24.25-27.5 GHz 4-channel dual-polarized ICs [11] have transmit (TX) and receive (RX) integrating a buffer, a phase shifter and a variable gain amplifier (VGA), with 8-bit phase and gain resolution.

C. Antenna Unit

The antenna element is a circular pin-fed stacked patch [10] as in the square-grid benchmark array with $0.5\lambda_0$ inter-element spacing, where λ_0 is the free-space wavelength at the center frequency f_0 of 26 GHz. Adopted from [11], a circular fence is used for isolation. A 64-element aperiodic array is synthesized by following the convex optimization algorithm proposed for minimization of side lobes (without mutual coupling considerations) [2]. The aperture size in the benchmark array in Fig. 1 is $3.5\lambda_0$ by $3.5\lambda_0$, while the proposed aperiodic one has an aperture of $4.3\lambda_0$ by $5\lambda_0$ due to sparsity on array edges.

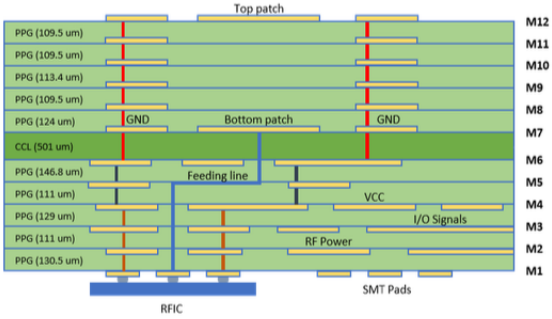

Fig. 2. 12-layer (M1-M12) substrate Astra MT77.

D. IC to Antenna Feeding Network

The ICs are distributed on M1 by following the k-means clustering algorithm [9], with several manual iterations for the feasibility. The transmission lines in the feeding network are designed to be similar to those in the reference array. On layer M5, a stripline is used to connect the IC RF pins with the corresponding feeding points of each patch. The stripline on layer M5 is surrounded by a ground on the same layer, and vias are used to connect to the upper and lower layers (M6 and M4) to prevent cross-talk with the striplines nearby. Additionally, a ground on layer M6 covers the entire stripline area to ensure isolation and proper grounding.

E. RF Signal Distribution Network

To distribute the RF signal from external connectors to the beamforming ICs, Wilkinson power dividers are used, ensuring high isolation among the ports while splitting the signal. Microstrip lines on M1 are primarily used for Vertical polarization (V-pol.), and striplines on M2 are used for most of the Horizontal polarization (H-pol.). A combination of the two transmission line structures allow for signal crossing when necessary and provide improved signal isolation. Since the lines for each IC channel have different lengths, calibration of the ICs will be necessary. However, by using the same number of Wilkinson splitters for each signal path and by adding meander lines to lengthen some short lines, the dynamic range of the amplitude calibration has been minimized.

F. Control Signals

The adaptive beamforming is set up using the beamformer IC gain and phase settings, which can be controlled through the Serial Peripheral Interface (SPI) through Low-Voltage Differential Signaling (LVDS) for fast communication. The ICs are divided into two groups of eight, each controlled by a Field-Programmable Gate Array (FPGA). The pins of an IC, the clock and data input and output signal connections, the chip select and the signals to determine the RF function of each channel are provided in [10]. The control lines are routed on layers M3 (mostly) and M2. The FPGA is located on the right side of the panel where all lines are routed.

G. Supply Network

The supply network is mostly on M4 and connected to the ICs through the copper areas on M3. To avoid undesired

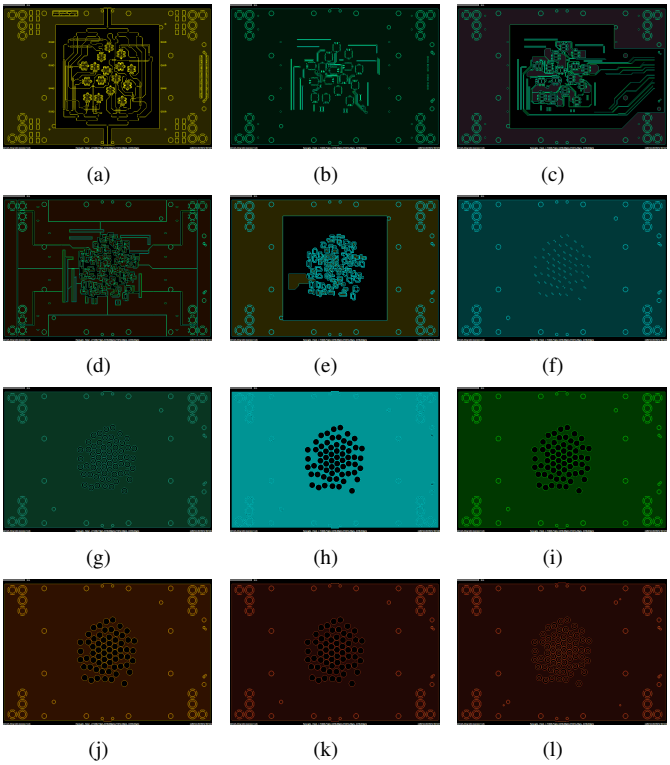

Fig. 3. Layer by layer panel view [10]: (a) M1, (b) M2, (c) M3, (d) M4, (e) M5, (f) M6, (g) M7, (h) M8, (i) M9, (j) M10, (k) M11, (l) M12.

capacitance from narrow lines, the copper layers are placed widely. The network is divided into 8 sections to reduce the noise. Each section feeds 4 ICs from 1 DC connector. The supplied voltage is kept within the upper and lower limits set on the ICs specifications, i.e. a maximum of 20 mV drop [10].

H. Panel Design

Complementary to the previous discussions, the 12 layers in the design are provided in Fig. 3. The two RF connectors are placed on the sides of the panel. The DC connectors for the supply are located on the corners, near the decoupling capacitors. Also, microFarad (around the array area) and nanoFarad (near the chips) capacitors are placed for docupling. The mechanics in the panel design (front casing, top frame, main PCB, bottom frame, FPGA board and heatsinks, interposers, stand and fan) are similar to the one in the reference array [11]. The top frame, main PCB and its interposer, bottom frame and thermal interfacing are updated to comply with the new dimensions.

I. Calibration

The measurements are conducted in the Delft University Chamber for Antenna Tests (DUCAT). Microwave Vision Group Open-Ended Waveguide (MVG OEW) 2200 is used as a near-field probe for IC-integrated embedded antenna response characterization in the Tx mode, based on the transmission coefficients (S_{21}) between the RF inputs and the probe. Due to the differences in line lengths from the RF inputs to the antenna element ports, load pull effects, temperature variations

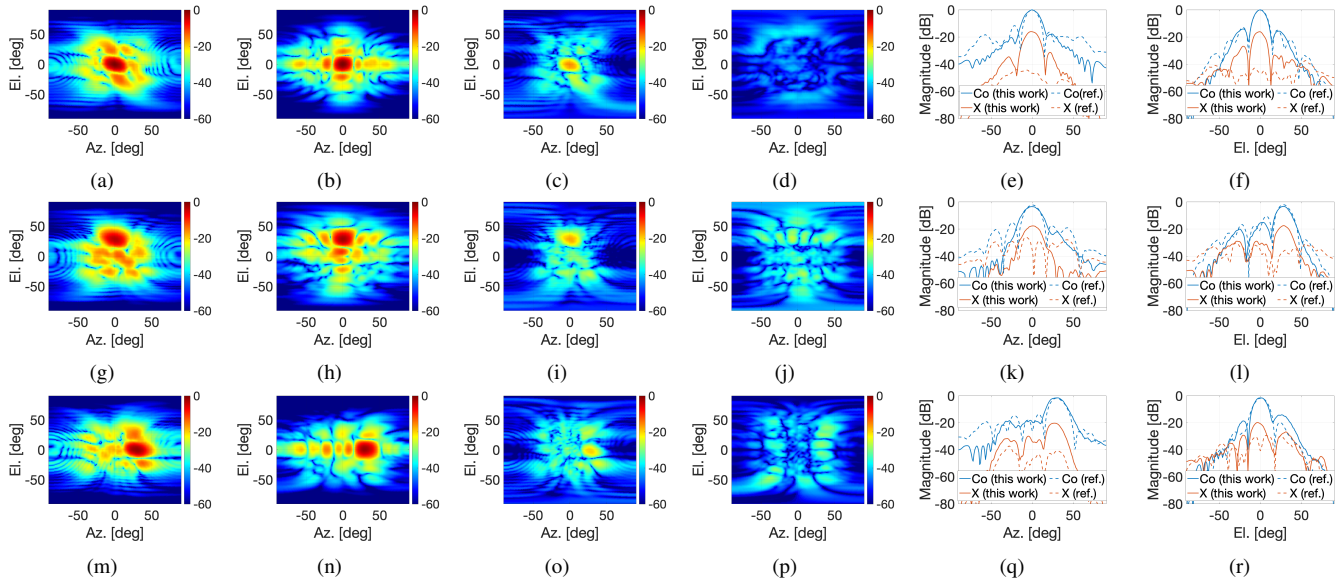

Fig. 4. Radiation patterns at 26 GHz in H-pol. mode: (a) [0 0] deg. scan, co-pol., this work, (b) [0 0] deg. scan, co-pol., ref., (c) [0 0] deg. scan, x-pol., this work, (d) [0 0] deg. scan, x-pol., ref., (e) [0 0] deg. scan, 0 deg. elevation, (f) [0 0] deg. scan, 0 deg. azimuth, (g) [0 30] deg. scan, co-pol., this work, (h) [0 30] deg. scan, co-pol., ref., (i) [0 30] deg. scan, x-pol., this work, (j) [0 30] deg. scan, x-pol., ref., (k) [0 30] deg. scan, 30 deg. elevation, (l) [0 30] deg. scan, 0 deg. azimuth, (m) [30 0] deg. scan, co-pol., this work, (n) [30 0] deg. scan, co-pol., ref., (o) [30 0] deg. scan, x-pol., this work, (p) [30 0] deg. scan, x-pol., ref., (q) [30 0] deg. scan, 0 deg. elevation, (r) [30 0] deg. scan, 30 deg. azimuth.

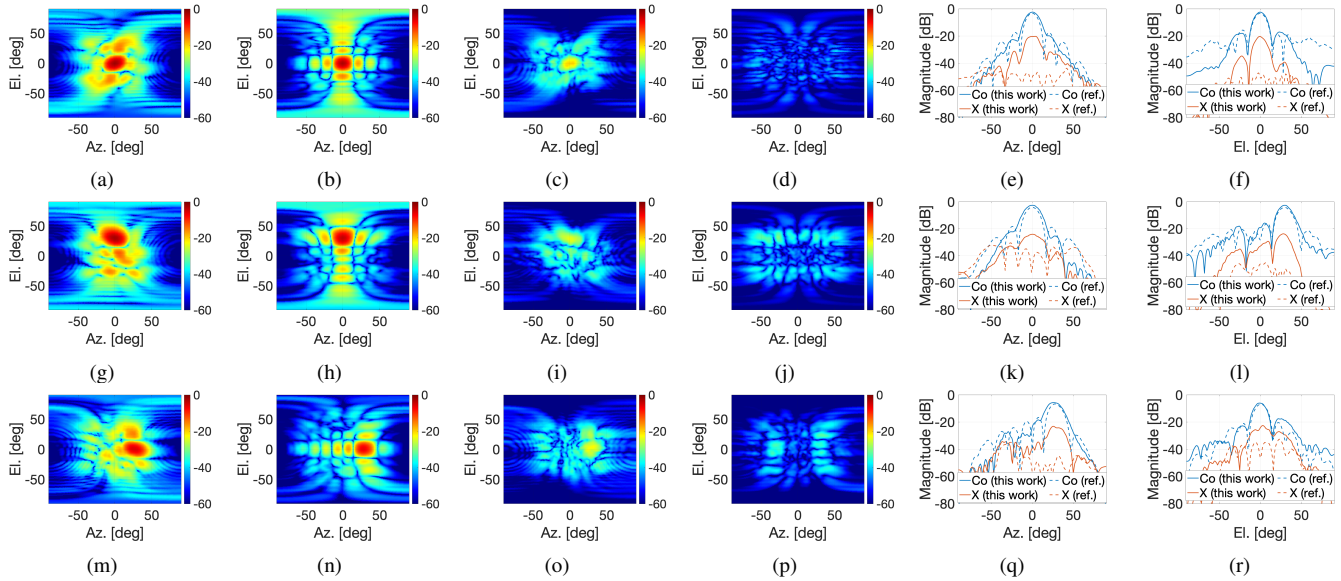

Fig. 5. Radiation patterns at 26 GHz in V-pol. mode: (a) [0 0] deg. scan, co-pol., this work, (b) [0 0] deg. scan, co-pol., ref., (c) [0 0] deg. scan, x-pol., this work, (d) [0 0] deg. scan, x-pol., ref., (e) [0 0] deg. scan, 0 deg. elevation, (f) [0 0] deg. scan, 0 deg. azimuth, (g) [0 30] deg. scan, co-pol., this work, (h) [0 30] deg. scan, co-pol., ref., (i) [0 30] deg. scan, x-pol., this work, (j) [0 30] deg. scan, x-pol., ref., (k) [0 30] deg. scan, 30 deg. elevation, (l) [0 30] deg. scan, 0 deg. azimuth, (m) [30 0] deg. scan, co-pol., this work, (n) [30 0] deg. scan, co-pol., ref., (o) [30 0] deg. scan, x-pol., this work, (p) [30 0] deg. scan, x-pol., ref., (q) [30 0] deg. scan, 0 deg. elevation, (r) [30 0] deg. scan, 30 deg. azimuth.

across the array and IC fabrication tolerances, the complex S_{21} responses for different gain-phase settings of the ICs vary for each channel. Here, the heuristic calibration method proposed in [13] is used, for H- and V-pol. activation separately at 26 GHz, which consists of the following steps:

- The probe is accurately positioned in front of each antenna element.
- $|S_{21}|$'s are measured sequentially for the same IC phase setting (equal to 0 in our case) at each element for varied IC gain settings from the maximal (= 255) to the minimal (= 0).
- New gain settings are calculated at each element to remove the $|S_{21}|$ discrepancies. The highest gain is given to the element with the largest feed line loss, which is nearly 20 dB higher than the loss in the reference array. This is done to achieve (nearly) uniform amplitudes to keep the paper focus on the comparison of array layouts. It is worth noting that decreasing RF signal distribution

Table 1. Radiation pattern performance of the aperiodic array in this work as compared to the referenced regular array.

	H-pol.								V-pol.							
Scan angle [deg-az. deg-el.]	**[0 0]**		**[0 30]**		**[30 0]**		**[30 30]**		**[0 0]**		**[0 30]**		**[30 0]**		**[30 30]**	
Cut-plane	**El.**	**Az.**	**El.**	**Az.**	**El.**	**Az.**	**El.**	**Az.**	**El.**	**Az.**	**El.**	**Az.**	**El.**	**Az.**	**El.**	**Az.**
Gain [dB]	/	/	-1.2	-1.2	+0.2	+0.2	-1	-1.5	+0.8	+0.8	+1.5	+1.5	+1	+1	+0.7	+0.8
HPBW [deg]	+3	n.c.	+4	n.c.	+4	n.c.	n.c.	n.c.	+3	n.c.	+4	n.c.	+4	n.c.	-1.5	-2
PSLL [dB]	-6	-1.2	-5.8	-3.3	-4.3	+6	-6.5	-4.3	-1.5	-2.2	-5.5	-1.5	-1	+3.8	-3.3	+2

Notes: The gain of each array is normalized with respect to its maximum at broadside. That is why the "/" sign is used for the gain at [0 0] degree scan in H-pol. mode. The "+" and "−" signs indicate increase and decrease, respectively. The abbreviation "n.c." denotes no change.

losses in the aperiodic layout via connector type and location optimization remains as future work.

- The phases of the transmission coefficients, after the amplitude correction, are measured one by one.
- The required linear phases for a given scan angle are determined based on the known element locations, and new phase settings are set by assuming 1.4-degree linear step size in the IC phase shifter settings.
- The IC settings are manually adjusted further for certain elements to achieve uniform amplitudes and linear phases as much as possible. The variations remain within ± 0.3 dB and ± 1 degree in all measurements as in the benchmark [13], which ensures a fair comparison.

III. Pattern Measurement Results

The radiation patterns of the proposed aperiodic array, with comparisons to the calibrated reference array results [13], are provided in Fig. 4 and Fig. 5 for H-pol. and V-pol. activation, respectively. 3 scan angles are considered: [0 0], [0 30], [30 0] degrees in the [azimuth (az.), elevation (el.)] representation. The results (including [30 30] degree scan) are summarized in Table 1 by considering the pattern performance (i.e. gain including the active components, half-power-beam-width (HPBW) and peak-side-lobe-level (PSLL)) at the two pattern cuts along the elevation and azimuthal planes. Based on these results, we can infer that:

- The PSLL is, in general, significantly (by up to 6.5 dB) lower in the aperiodic array, except for a few cases such as azimuthal cut-plane for [30 0] degree scan. The differences in different polarization modes and cut-planes originate from the varying mutual coupling.
- The HPBW is, in general, similar in the two arrays, except for the slight increase (by up to 4 degrees) in the azimuthal cut-plane of the aperiodic array patterns.
- For the aperiodic array, the scan loss is improved (by 1 dB on average) in the V-pol. case, while it is worse (by 0.75 dB on average) in the H-pol. mode.
- Due to the asymmetry in the feeding network, the cross-polarization (x-pol.) levels are significantly higher in the aperiodic array (except for the diagonal scanning).

IV. Conclusion

A first-of-its-kind active phased array with an aperiodic IC and antenna layout is developed. Circuit routing with the multi-channel dual-polarized ICs is designed. The novel array system is prototyped and experimentally verified. A heuristic calibration procedure is applied to achieve close-to-uniform amplitudes and linear phases at the elements. It is demonstrated that the aperiodic array topology is, in general, useful to suppress the PSLL without significant changes in the scan loss and HPBW. The open challenges, and future work, include reducing the losses in the feed network, decreasing the cross-polarization levels and dealing with the coupling.

Acknowledgment

The authors would like to thank the Radar Technology department of Netherlands Organisation for Applied Scientific Research (TNO) for the development of the antenna element.

References

[1] G. Toso, P. Angeletti, and C. Mangenot, "A comparison of density and amplitude tapering for transmit active arrays," in *Proc. EuCAP*, 2009, pp. 840–843.

[2] Y. Aslan, J. Puskely, A. Roederer, and A. Yarovoy, "Multiple beam synthesis of passively cooled 5G planar arrays using convex optimization," *IEEE Trans. Antennas Propag.*, vol. 68, no. 5, pp. 3557–3566, 2020.

[3] K. K. W. Low, G. M. Rebeiz, S. Zihir, and T. Kanar, "A reconfigurable dual-polarized 1024-element Ka-band satcom transmit phased-array with large scan volume and +48 dBW EIRP," in *Proc. IEEE MTT-S IMS*, 2021, pp. 638–640.

[4] E. V. P. Anjos *et al.*, "Format: A reconfigurable tile-based antenna array system for 5G and 6G millimeter-wave testbeds," *IEEE Sys. J.*, vol. 16, no. 3, pp. 4489–4500, 2022.

[5] M. Kohtani *et al.*, "Thinned array with steerable nulls to cancel grating lobe for automotive radar applications," in *Proc. EuMC*, 2022, pp. 385–388.

[6] M. Repeta *et al.*, "A scalable 256-element e-band phased-array transceiver for broadband communications," in *Proc. IEEE/MTT-S IMS*, 2020, pp. 833–836.

[7] A. J. van den Biggelaar *et al.*, "On the design and calibration of a 5G millimeter-wave dual-polarized active phased array," in *Proc. IEEE-APS APWC*, 2021, pp. 55–60.

[8] J. R. De Luis *et al.*, "Antenna-to-beamformer assignment and mapping in phased array antenna systems," 2021, US Patent 10,971,817.

[9] Y. Aslan, J. Puskely, A. Roederer, and A. Yarovoy, "Synthesis of quasi-modular circularly polarized 5G base station antenna arrays based on irregular clustering and sequential rotation," *Microw. Opt. Technol. Lett.*, vol. 63, no. 4, pp. 1278–1285, 2021.

[10] M. Buenaventura Camps, "Design of a sparse irregular array for beyond 5G base stations," *MSc Thesis, TU Delft, The Netherlands*, 2021.

[11] M. Geurts and J. Janssen, "Designing a 5G mm-wave antenna means balancing tradeoffs," 2023, NXP Smarter World Blog.

[12] A. Garufo *et al.*, "Mm-wave antennas in package for 5G applications," in *Proc. IEEE ISAP*, 2021.

[13] Y. Aslan *et al.*, "Heuristic over-the-air calibration of beamformer ICs in active mm-wave phased arrays," in *Proc. IEEE CAMA*, 2023, pp. 840–845.